

# Green Chemistry

Accepted Manuscript



This is an *Accepted Manuscript*, which has been through the Royal Society of Chemistry peer review process and has been accepted for publication.

*Accepted Manuscripts* are published online shortly after acceptance, before technical editing, formatting and proof reading. Using this free service, authors can make their results available to the community, in citable form, before we publish the edited article. We will replace this *Accepted Manuscript* with the edited and formatted *Advance Article* as soon as it is available.

You can find more information about *Accepted Manuscripts* in the [Information for Authors](#).

Please note that technical editing may introduce minor changes to the text and/or graphics, which may alter content. The journal's standard [Terms & Conditions](#) and the [Ethical guidelines](#) still apply. In no event shall the Royal Society of Chemistry be held responsible for any errors or omissions in this *Accepted Manuscript* or any consequences arising from the use of any information it contains.



[www.rsc.org/greenchem](http://www.rsc.org/greenchem)

## ARTICLE

# One-pot synthesis of B-doped three dimensional reduced graphene oxide via supercritical fluid for oxygen reduction reaction

Cite this: DOI: 10.1039/x0xx00000x

Received 00th,  
Accepted 00th

DOI: 10.1039/x0xx00000x

[www.rsc.org/](http://www.rsc.org/)Yazhou Zhou,<sup>ab</sup> Clive Hsu Yen,<sup>c</sup> Shaofang Fu,<sup>a</sup> Guohai Yang,<sup>a</sup> Chengzhou Zhu,<sup>a</sup> Dan Du,<sup>a</sup> Pui Ching Wo,<sup>a</sup> Xiaonong Cheng,<sup>b</sup> Juan Yang,<sup>\*b</sup> Chien M. Wai,<sup>c</sup> and Yuehe Lin<sup>\*a</sup>

There has been a great deal of interest recently in three-dimensional (3D) graphene based materials, as they exhibit large surface areas, unique electronic properties, and other attractive features. Particularly, 3D graphene doped with heteroatoms catalysts show high electrocatalytic activity toward oxygen reduction reaction (ORR), which can be used as metal-free catalysts. Most of the existing synthesis strategies of 3D graphene invariably involve multiple steps and procedures are often energy intensive and time-consuming. In this paper, we reported a one-pot and green method to synthesize boron-doped 3D reduced graphene oxide (B-3DrGO) using supercritical carbon dioxide (ScCO<sub>2</sub>) technique. The resultant products exhibit hierarchical porous structures, leading to a high specific surface area of 541 m<sup>2</sup> g<sup>-1</sup>. A high content of B (2.9 at%) was detected in the product, suggesting the B-doping was efficient using this technique. The B-3DrGO displays electrocatalytic activity toward ORR, that is comparable to the commercially available Pt/C (20 wt.%) catalyst, in addition to their superior durability and resistance to crossover effect. Moreover, supercritical fluid technique, which uses non-flammable, essentially nontoxic, inexpensive, and environmentally benign CO<sub>2</sub>, is a new and green approach for synthesis of heteroatoms doped 3D graphene.

## 1. Introduction

Graphene, a two-dimensional and conjugated honeycomb carbon network, has attracted increasing attentions due to their exceptionally unique properties.<sup>1</sup> Unfortunately, the unavoidable restacking and agglomeration caused by van der Waals interactions in graphene based materials significantly diminish their surface area and electrical conductivity. Three-dimensional (3D) graphene, featured a pore-rich and perfect sheet-to-sheet connectivity, exhibits accessible surface area, high electrical conductivity,<sup>2</sup> high corrosion resistance, and efficient mass transfer, thus it opens up new opportunities for potential applications in supercapacitors,<sup>3</sup> batteries,<sup>4</sup> photovoltaic cells,<sup>5</sup> hydrogen storage,<sup>6</sup> and fuel cells.<sup>7</sup> One of the major hurdles for wide applications of graphene based materials lies in the difficulty in efficient mass production of such materials that have the advantageous microstructure as well as desirable properties.

3D graphene can be produced by a number of methods, such as chemical vapour deposition (CVD),<sup>8</sup> physical/chemical assemblies,<sup>9-</sup>

<sup>11</sup> unidirectional freezing and freeze-drying of bare graphene oxide (GO) suspension,<sup>12</sup> self-assembly,<sup>13-15</sup> and direct-grow.<sup>16</sup> However, these strategies usually involve multiple steps in order to obtain a material that exhibits an optimum combination of physical, mechanical, thermal and electrical properties suitable for energy generation and/or storage devices. For example 3D graphene structure in the form of a graphene aerogel can be obtained from first drying the graphene hydrogel either using a freeze-dryer or a supercritical carbon dioxide (ScCO<sub>2</sub>) drying technique.<sup>17</sup> In order to achieve the preferred electrical conductivity, the graphene aerogels will then have to undergo a reduction process through thermal annealing.<sup>18</sup> Each of these manufacturing steps is independently crucial, but they are also inter-dependent. Because of these, the synthesis of 3D graphene that possesses particular desirable properties has been inevitably labor intensive, time-consuming and require considerable energy consumption.<sup>19</sup> This study aims to explore the possibility of a simple one-pot strategy to manufacture 3D graphene using ScCO<sub>2</sub> technique.

The ScCO<sub>2</sub> technique has traditionally been used during the synthesis and processing of nanoscale particles,<sup>20</sup> wires,<sup>21</sup> films,<sup>22</sup>

and other high-quality porous materials.<sup>23</sup> Only recently, ScCO<sub>2</sub> has been used for the intercalation and exfoliation of graphite structure during the preparation of few-layer graphene sheets.<sup>24</sup> Generally, ScCO<sub>2</sub> has much more empty space than ordinary liquids and so it is highly compressible. This characteristic allows the solvent strength of the liquid phase ScCO<sub>2</sub> be 'adjustable' between gas-like and liquid-like by simply varying the operating pressure and/or temperature.<sup>20,25</sup> In addition, the low viscosity, zero surface tension, excellent surface wetting property and high diffusivity of ScCO<sub>2</sub> make it a potential candidate as a superior solvent for the manufacturing of graphene as it can diffuse in between and expand graphite layers. Most of the current synthesis routines for 3D graphene use ScCO<sub>2</sub> technique only during the step of drying hydrogel to aerogel for keeping the porous structure. ScCO<sub>2</sub> technique, however, has not been as a technique for direct synthesis of 3D graphene.

Moreover, great improvements in the electrochemical activity, selectivity and durability have been evidently shown in graphene doped with heteroatoms, such as nitrogen (N),<sup>26</sup> boron (B),<sup>27</sup> halogen (Cl, Br, I),<sup>28</sup> phosphorus (P),<sup>29</sup> sulfur (S)<sup>30</sup> and mixtures of different heteroatoms,<sup>31</sup> opening up the potential application in fuel cell as metal-free catalysts for oxygen reduction reaction (ORR). In particular, considerable studies had been carried out on graphene doped with N and B. The similarities of atomic mass and size of these heteroatoms to those of C made them suitable dopants in the carbon lattice. N and B are exceptional dopants in C-based materials since their electron configurations allow electrons or holes to be injected easily, which can alter the overall electronic and transport properties of these doped graphene materials.<sup>32</sup>

In this study, we introduce a novel and green approach of using ScCO<sub>2</sub> technique to directly synthesize a 3D-structured B-doped reduced graphene oxide (B-3DrGO). This new technique is distinctly superior to the existing manufacture process because 1) it is a 'one-pot' method with a relatively simple set-up; 2) the reducing agent can be completely removed from the product simply through the release of CO<sub>2</sub> and so no additional cleaning and drying processes are required; 3) ScCO<sub>2</sub> is non-flammable, essentially nontoxic, inexpensive, and environmentally benign. The resultant B-3DrGO exhibits hierarchical porous structure that leads to a high specific surface area. More importantly, excellent electrocatalytic activity toward ORR, outstanding stability and durability to methanol are also observed in the newly synthesized B-3DrGO product.

## 2. Experimental

### 2.1 Materials

Tetrahydrofuran (THF), Borane tetrahydrofuran complex solution, 1.0 M in THF (Borane-THF), Borane triethylamine complex (97%, Borane-N(C<sub>2</sub>H<sub>5</sub>)<sub>3</sub>), methanol, isopropanol (99.5%), Nafion (5%) were all purchased from Sigma-Aldrich. Potassium hydroxide (KOH, 80-90 wt.%) were purchased from J.T. Baker Chemical Co. Commercial platinum/carbon (Pt/C) (Pt loading: 20 wt.%, Pt on carbon black) was purchased from Alfa Aesar. Graphite oxide (GO) was prepared from purified natural graphite by the modified Hummers method<sup>33</sup> and was freeze-dried.

### 2.2 Safety Warning

Operators of high-pressure equipment such as that required in the experiments described hereafter should take proper precautions,

including, but not limited to, the use of blast shields and pressure relief mechanisms, in order to minimize the risk of personal injuries.

### 2.3 Syntheses of B-3DrGO

Typically, freeze-dried GO powder (10 mg) was added into 0.5 mL THF, followed by sonication for 2 h. Then, 0.5 mL of a selected reducer was added into the GO/THF complex. Two types of reducers, borane-THF and borane-N(C<sub>2</sub>H<sub>5</sub>)<sub>3</sub>, were used in this study, leading to the formation of two different products. This GO/THF complex and the selected reducer were transferred into a 10 mL reaction cell located in an oven heated to 313 K. After that, the CO<sub>2</sub> was pumped into the reaction cell until the pressure reached to 150 atm. The temperature of the reaction cell was then increased and maintained at 353 K. Meanwhile, the cell pressure increased to 300 atm because of increased temperature. After 24 h, the system was cooled down slowly to 333 K before it was depressurized by the release of CO<sub>2</sub> from the cell. The product was then washed by a continuous feed of 80 mL of CO<sub>2</sub> and released at a rate of ~ 0.5 mL min<sup>-1</sup>. Finally, the washed product was collected when all the CO<sub>2</sub> is released. The two products prepared by using different reducers, i.e. borane-N(C<sub>2</sub>H<sub>5</sub>)<sub>3</sub> and borane-THF were labelled as B1-3DrGO and B2-3DrGO, respectively. For comparison, two controlled samples were prepared. One is B-doped graphene (B-rGO) prepared using a solution process according to Han et al.<sup>34</sup> The second one is 3DrGO without B-doping, which was manufactured using the proposed process described above, but H<sub>2</sub> was used as the reducer.

### 2.4 Characterizations

The morphologies of the products were characterized using a FEI Sirion field emission gun scanning electron microscope (SEM) operated at 10-12 kV. Secondary electron images were obtained using a through-the-lens (TLD) detector. The X-ray diffraction (XRD) analyses were performed on a Siemens D5000 powder X-ray diffractometer using Cu KR radiation generated at 40 kV and 30 mA. The X-ray photoelectron spectroscopy (XPS) analyses were performed on a Kratos AXIS-165 with a monochromatized AlK $\alpha$  X-ray anode (1486.6 eV). The scanning confocal Raman microscope system was a WITec Alpha300 (WITec Instruments Corp., Ulm, Germany). The laser excitation wavelength was 532 nm and the optical magnification at the objective was 20  $\times$ , producing a spot size of roughly 2.5  $\mu$ m in diameter. Nitrogen adsorption-desorption measurements were performed on a Quantachrome autosorb-6 automated gas sorption system to study the porous structure and measuring the surface area of the products.

### 2.5 Electrochemical Characterizations

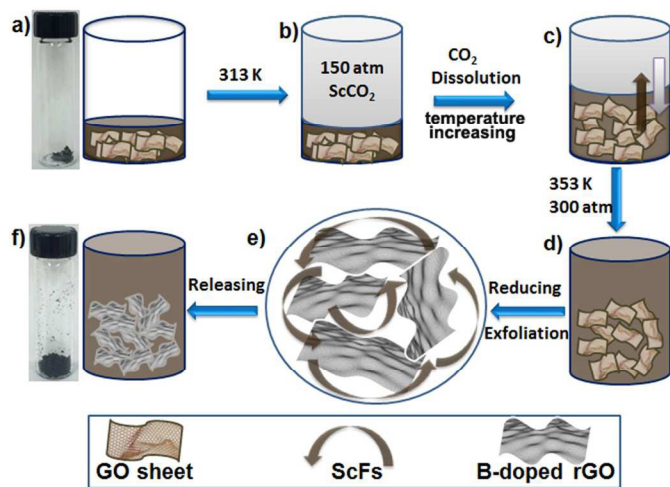
The electrochemical tests were carried out in a standard three electrode system controlled by a CHI 630E station (CH Instruments, Inc., USA). A Pt wire and a Ag/AgCl were used as the counter electrode and the reference electrode, respectively. The working electrodes were pre-polished glassy carbon (GC) disk electrodes (5 mm in diameter) with catalyst inks applied on them. In brief, to prepare the catalyst inks, the as-prepared electrocatalyst was dispersed in a mixture of isopropanol (99.5%), Nafion (5%), water (V/V/V: 2/0.05/8), which was ultrasonicated to form a uniform catalyst ink (2 mg mL<sup>-1</sup>). 10  $\mu$ L of well dispersed catalyst ink was used in each working electrodes. These electrodes were then dried at 60 °C for 30 min before they were used in the electrochemical tests. For comparison, catalytic performance of commercially available Pt/C (20 wt. % Pt) was also investigated under the same condition. In addition, all the samples were uniformly dispersed on the glassy

carbon disk electrodes. Care was taken to ensure similar coverage of samples on each working electrode.

### 3. Results and discussion

#### 3.1 Preparation and characterization of B-3DrGO product

The scheme of the proposed synthesis strategy of B-3DrGO (described in experimental section) is shown in Scheme 1. It is well-known that the reactions in supercritical fluids (SCFs) can be strongly affected by the phase of the content. Thus, the phase behaviour of system should be firstly determined. According to the literature, the solubility of THF and  $N(C_2H_5)_3$  in  $ScCO_2$  are very high, even higher than these of methanol and ethanol. Thus, a single phase can be achieved when mixing  $ScCO_2$  and THF or  $N(C_2H_5)_3$  under certain temperatures and pressures.<sup>36,37</sup> In this experiment, borane-THF or borane- $N(C_2H_5)_3$  were used as the reducer; the borane that released from the complex is in a gaseous state, which does not affect the solubility of THF or  $N(C_2H_5)_3$  in  $ScCO_2$ . As shown in Scheme 1a, this illustration begins with a liquid phase that contains GO/THF colloid in either borane-THF or borane- $N(C_2H_5)_3$ . Then, a SCF phase ( $ScCO_2$ ) is introduced into the liquid phase (Scheme 1b). According to our prior experiences, a single phase can only be achieved when the volume of the liquid solvent is less than 10% of the total volume of the cell. As the temperature increases, the dissolution of  $CO_2$  will create the turbulence in the liquid phase, leading to an expansion of the liquid volume<sup>35</sup> and consequently increases the system pressure. This expansion of liquid volume causes the GO sheets to be further apart from each other and hence there is a larger space between them (Scheme 1c). A single phase is achieved when the liquid phase was completely mixed with  $ScCO_2$  at 353 K and 300 atm (Scheme 1d).<sup>36,37</sup> Under these conditions, the GO sheets are exfoliated by the fluids and at the same time they are also being reduced and doped by the reducing agent (Scheme 1e). Finally, the B-3DrGO is obtained (Scheme 1f).



**Scheme 1.** Schematic illustration for the synthesis of B-3DrGO. The phase behavior of the borane-THF or borane- $N(C_2H_5)_3$ /THF/ $ScCO_2$  system in a 10-mL reaction cell is shown.

The products were examined in the SEM in order to verify whether a 3D structure is obtained. It can be seen in the SEM image that the B2-3DrGO produced from borane-THF reducing agent has a well-defined 3D porous network structure (Fig. 1a and Fig. 1b). The pores are more or less equiaxed in shape with a diameter in the order

of 10s of micrometer, and appear to be formed from the curling of sheets with some ripples on the surface. As discussed in the experimental section, the GO sheets in the highly concentrated GO colloid (10 mg/mL) aggregated to form a GO gel that could potentially in the form of a 3D framework structure. The unique features of the SCFs, such as low viscosity, excellent wetting of surfaces, high solvation power and high diffusivity allow them to rapidly penetrate in between individual GO interlayers (Scheme 1e), forming an expanded framework structure. Moreover, the rGO sheets are not smooth but are covered with wave-like nanometer-sized ripples (Fig. 1c and 1d). The vigorous reducing reactions between the GO sheets and borane, together with the intercalation and exfoliation by SCFs may have created and wrinkled the GO sheets and lead to such wave-like ripples. In addition, all the SCFs can be removed through the release of  $CO_2$ . Thus, the 3D porous structure can be preserved because no liquid solvent washing is required. The above SEM examination demonstrates that a hierarchical structure that involves multi-scale morphological features including pores in the order of 10s micrometer and the nanometer-sized ripples on the surface of the rGO layers was achieved in the B2-3DrGO product. The nanometer-sized ripples help in preventing the restacking of overlapping rGO sheets, and they lead to the large surface area.<sup>16,38</sup> Similar morphologies were observed in the B1-3DrGO product.

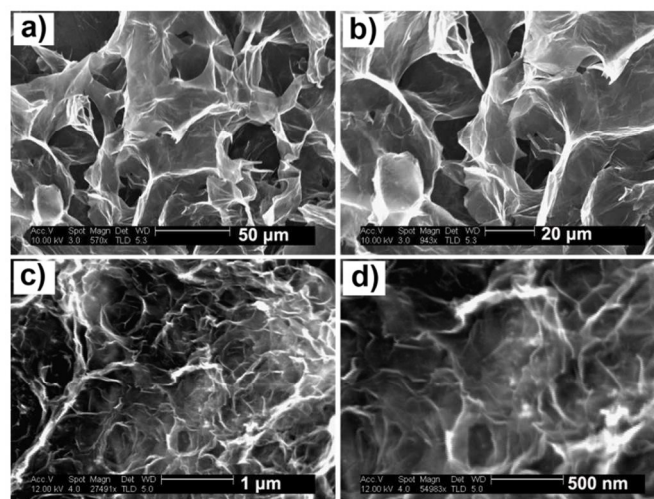


**Fig. 1.** SEM images showing morphology of the B2-3DrGO product. (a) and (b) well-defined 3D porous structure can be observed at low magnification. (c) and (d) ripples can be seen on surface of rGO layers at high magnification.

As discussed above, the porous network structure of the products is likely the result of exfoliation and expansion of the rGO due to the action of SCFs. The initial GO concentration is then another crucial deterministic factor for the formation of the porous 3D network morphology. In this study, porous network structure was not observed in product prepared using a lower ( $5 \text{ mg mL}^{-1}$ ) or higher ( $15 \text{ mg mL}^{-1}$ ) GO concentration (Fig. S1a†). When the GO concentration is  $15 \text{ mg mL}^{-1}$ , a large bulk of flake-like rGO sheets was observed (Fig. S1b†). This may be because of the much smaller space available for the diffusion of SCFs as the GO concentration increased. The lack of SCFs diffusion could not exfoliate and expand the overlapping and/or coalescing graphene sheets. When the GO concentration is  $5 \text{ mg L}^{-1}$ , although there is larger space between the GO sheets for diffusion of SCFs, 3D network was not achieved except abundant ripple structures. These observations suggest that the formation of the 3D network has a strong

dependence on the GO concentration, whereas the SCFs and reduction reaction play important roles in the formation of the porous network and ripple structures.

The hierarchical porous structures of B2-3DrGO product observed from the SEM images were further characterized using the N<sub>2</sub> adsorption-desorption measurements. The result shown in Fig. 2a exhibits the IUPAC type-IV isotherm. The temporary locking of liquid N<sub>2</sub> and the delayed evaporation in the desorption isotherm indicate the product behaves similar to the type H3 hysteresis loops, implying the abundant presence of hierarchical pores. The steep increases of N<sub>2</sub> uptake at low pressure and the hysteresis loop at high pressure are both characteristics for the presence of micro-, meso- and macro-porous structures. The pore distribution obtained using the Barret-Joyner-Halenda (BJH) theory indicates that the width of the pores were 1-5 nm (meso-pores) and 28 nm (micro-pores) (Fig. 2b). The N<sub>2</sub> adsorption-desorption results are in good agreement with the SEM observations. The meso- and micro-pores are attributed to the ripples on the rGO sheets mentioned above. This explains the high specific surface area of 541 m<sup>2</sup> g<sup>-1</sup> and the large total pore volume of 0.73 cm<sup>3</sup> g<sup>-1</sup> determined from the Brunauer-Emmett-Teller (BET) analysis. The B1-3DrGO and the B2-3DrGO samples show similar N<sub>2</sub> adsorption-desorption behaviour (Fig. S2<sup>†</sup>). However, a smaller specific surface area (535.4 m<sup>2</sup> g<sup>-1</sup>) and a lower total pore volume (0.65 cm<sup>3</sup> g<sup>-1</sup>) were observed in the B2-3DrGO sample.

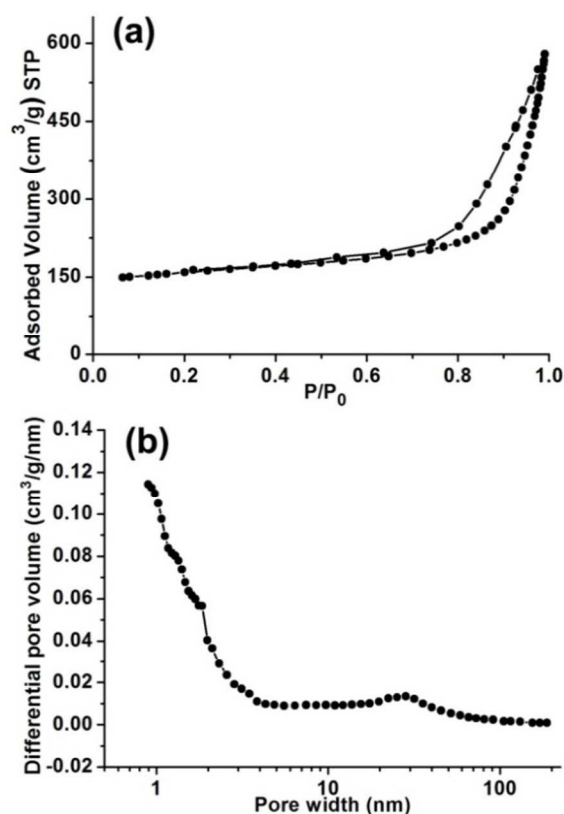


**Fig. 2.** (a) Nitrogen adsorption/desorption isotherms and (b) pore size distribution in B2-3DrGO.

The structure of the B-3DrGO products was further characterized using XRD. The corresponding XRD patterns (Fig. 3) show an apparent structural change when the GO sheets were reduced by borane-THF or borane-N(C<sub>2</sub>H<sub>5</sub>)<sub>3</sub>. The XRD pattern of the GO exhibits a typical strong (002) peak at  $2\theta=10.3^\circ$ ,

corresponding to an interlayer spacing of 8.6 Å. This large interlayer distance is attributed to the presence of the hydroxyl, epoxy, and carboxyl groups. After the removal of such functional groups through the reduction process the interlayers will get closer to each other, resulting in a smaller interlayer spacing. It is found that the interlayer distance for B1-3DrGO prepared using borane-N(C<sub>2</sub>H<sub>5</sub>)<sub>3</sub> as a reducing agent is 3.80 Å ( $2\theta=20.4^\circ$ ). A smaller interlayer distance is measured for B2-3DrGO ( $d=3.73$  Å,  $2\theta=21.6^\circ$ ) prepared using borane-THF. Interlayer spacing of both products are larger than that of natural graphite ( $d=3.36$  Å,  $2\theta=26.5^\circ$ ), suggesting the existence of functional groups in both products. The smaller interlayer spacing observed in B2-3DrGO indicates that more functional groups were removed from the GO sheets by the stronger reducer, borane-THF and that the resulting rGO sheets underwent larger degree of reduction.

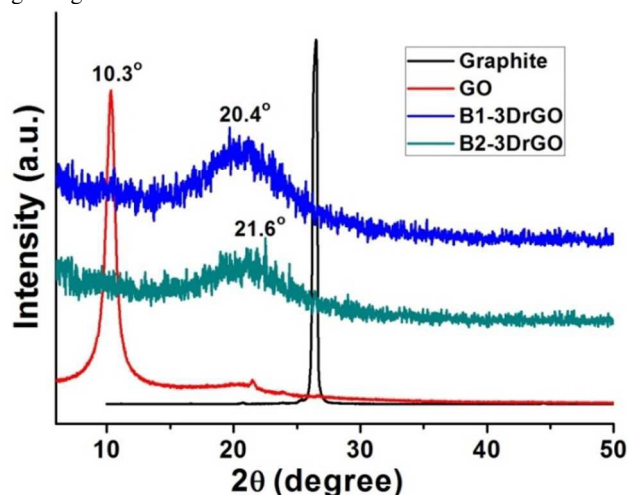


**Fig. 3.** XRD patterns of B1-3DrGO and B2-3DrGO products. The patterns for graphite and GO are included for comparison.

XPS characterization was carried out to explore the extent of the reduction of the GO sheets, and the content and configuration of the boron doping in the rGO structure. In the C1s XPS spectrum of GO, four clear peaks are assigned to the four types of carbon having different chemical valences: non-oxygenated ring C (C=C/C-C), hydroxyl (C-O), epoxy (C-O-C) and carbonyl (C=O, O-C=O) (Fig. S3<sup>†</sup>).<sup>39</sup> After reduction, the intensities of the oxygen functionality peaks, especially the C-O-C groups, in the C1s XPS spectra of both B-3DrGO products noticeably decrease, indicating a high degree of reduction in the products (Fig. 4a and 4b). The C/O ratios of the GO sheets significantly increase from 1.3 to 4.5 and 5.9 for B1-3DrGO and B2-3DrGO, respectively (Table S1<sup>†</sup>). The corresponding high-resolution B 1s spectra obtained from B1-3DrGO (Fig. 4c) and B2-3DrGO (Fig. 4d) can be deconvoluted into the B-C and the B-O peaks located at around 190.2 eV and 191.3 eV, respectively, with the B-O being the dominating component.<sup>40</sup> These results suggest that the B atoms were doped into the rGO layers through a reaction between the oxygenated functional group and borane. Additionally, the noticeable B-C peaks, which can also be found in both products, indicate that some B atoms have been successfully incorporated into the graphene lattice network. The boron content is 2.1% (at%) for B1-3DrGO and 2.9% for B2-3DrGO. These values are much higher than 1.1%, which was obtained from B-rGO prepared using a solution process (Table S1<sup>†</sup>). The XPS results show that the B2-3DrGO product prepared using borane-THF has a higher reduction degree and a higher B content compared to the B1-3DrGO product. It had been shown that, a high B content and the presence of B-C chemical band can significantly improve the electrocatalytic activity toward ORR as they both provide numerous catalytic sites.<sup>41</sup> Thus

B2-3DrGO is expected to have a higher electrocatalytic activity compared to B1-3DrGO.

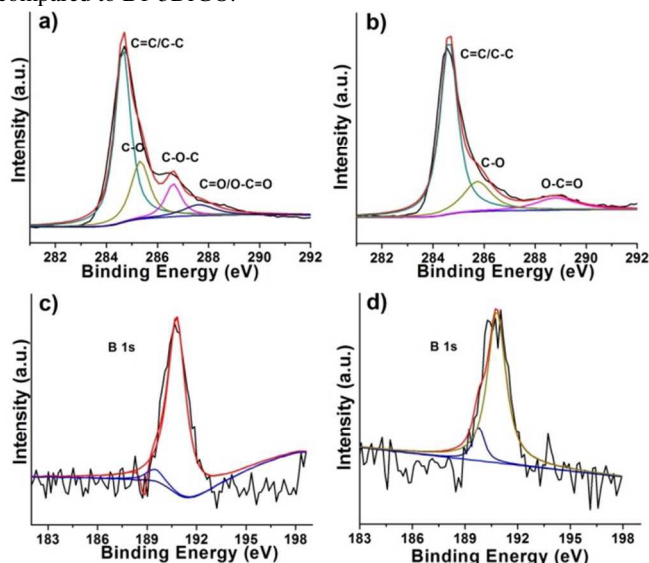


**Fig. 4.** XPS C 1s spectra of (a) B1-3DrGO and (b) B2-3DrGO. XPS B 1s spectra of (c) B1-3DrGO and (d) B2-3DrGO.

Raman spectroscopy is one of the most effective and non-destructive techniques to characterize the structure and quality of carbon materials. The Raman spectra of the as-prepared B1-3DrGO, B2-3DrGO and GO are shown in Fig. 5. The D band at approximately  $1,348\text{ cm}^{-1}$  indicates the presence of defects caused by the  $\text{sp}^3$ -hybridized carbon atoms, while the pristine  $\text{sp}^2$  lattice carbon atoms in the graphene sheet shows a G band at approximately  $1,600\text{ cm}^{-1}$ .<sup>42</sup> The ratio between D and G band intensities ( $I_D/I_G$ ) can be used as an indication of the degree of disorder in a carbon structure. It has been shown that B doping into rGO layers could break the hexagonal symmetry of graphite, inducing a higher D band intensity in the Raman spectrum.<sup>41</sup> As shown in the Raman spectra, the  $I_D/I_G$  ratio significantly increases from 0.96 for GO to 1.25 for B1-3DrGO after reduction. This indicates that there is an increase in the number

of defects in the B1-3DrGO sheets likely due to the strong reduction and the B doping during the  $\text{ScCO}_2$  treatment. Furthermore, the distinct second-order Raman band (2D band) located around  $2,670\text{ cm}^{-1}$  can be observed from the B1-3DrGO spectrum, confirming that this product exhibits a graphitic structure having only a few layers. The 2D band in the spectrum for B2-3DrGO is significantly smaller and the  $I_D/I_G$  is higher (1.44) compared with that of B1-3DrGO. These results suggest that B2-3DrGO has more defects in the rGO layers than those in the B1-3DrGO. It can be concluded from the XRD and XPS results that there is a higher population of defects in the B2-3DrGO sheets, which can be attributed to the stronger reducing activity of borane-THF that leads to an efficient B doping within the carbon hexagonal lattice under the  $\text{ScCO}_2$  environment.

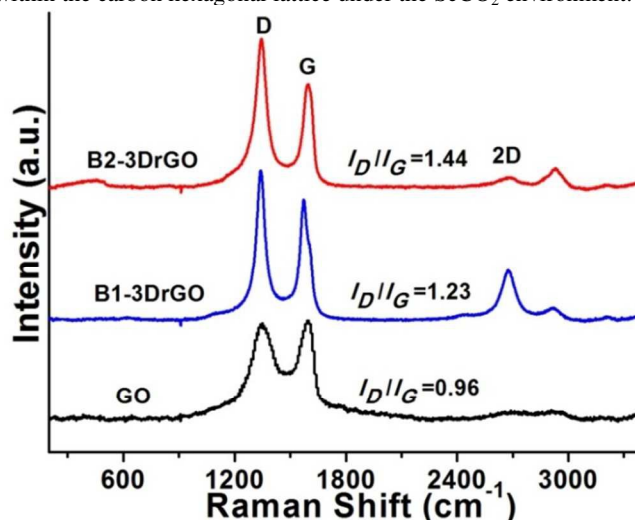


**Fig. 5.** Raman spectra of GO, B1-3DrGO and B2-3DrGO.

### 3.2. Electrochemical performance of the B-3DrGO product.

Having characterized the morphological and the chemical structures of the B-3DrGO products, their electrocatalytic activities in 0.1 M KOH solutions were investigated. In particular, we compared the electrocatalytic activities toward ORR for B-3DrGO, undoped 3DrGO, B-rGO and a commercial Pt/C (20 wt.%) by means of cyclic

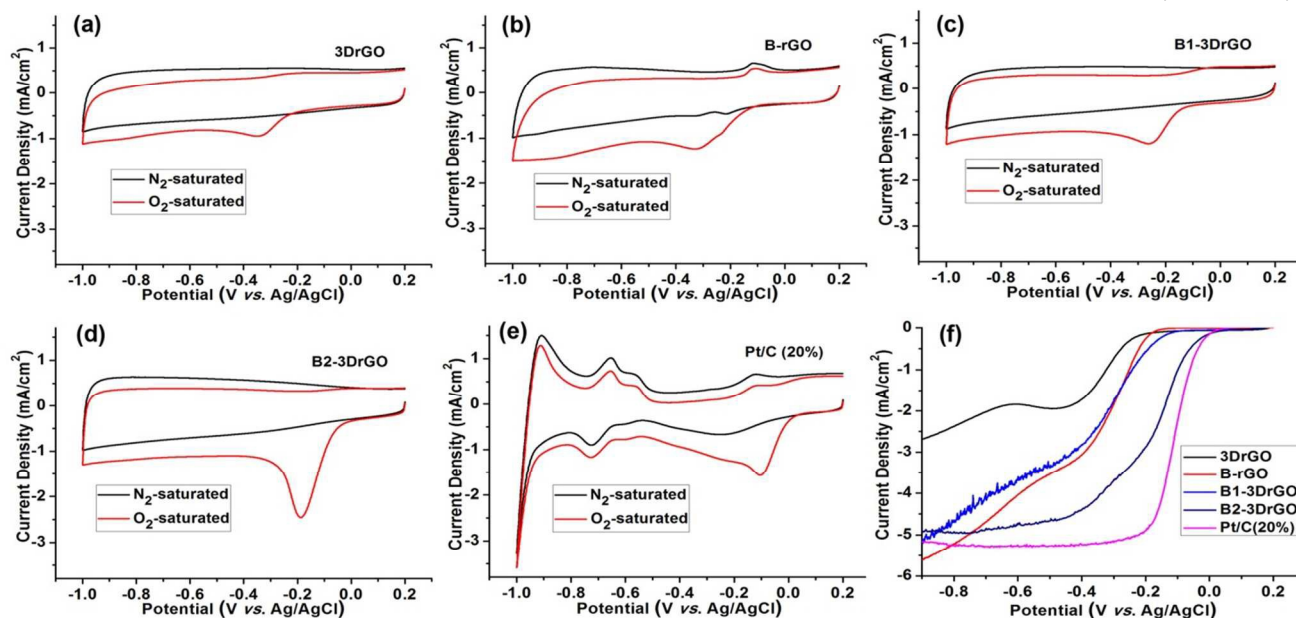


**Fig. 6.** CVs of samples on GC electrodes in  $\text{N}_2$ - and  $\text{O}_2$ -saturated 0.1 M KOH solution with a scan rate of  $50\text{ mV s}^{-1}$ . (a) 3DrGO, (b) B-rGO, (c) B1-3DrGO, (d) B2-3DrGO and (e) commercial Pt/C (20 wt.%). (f) ORR polarization curves of aforementioned samples at a rotation rate of 1600 rpm and a scan rate of  $10\text{ mV s}^{-1}$ .

voltammetry in an aqueous solution of  $N_2$ -saturated or  $O_2$ -saturated 0.1 M KOH solution at a scanning rate of  $50 \text{ mV s}^{-1}$  (Fig. 6). As shown in Fig. 6(a-e), all five electrodes show a substantial oxygen reduction peaks in the  $O_2$ -saturated 0.1 M KOH solution, while displaying featureless cyclic voltammograms (CVs) in the corresponding  $N_2$ -saturated medium. Fig. 6a shows a single cathodic reduction peak at  $-0.36 \text{ V}$  with a current density of  $-0.92 \text{ mA cm}^{-2}$  for the 3DrGO electrode. The corresponding cathodic reduction peaks for the B-rGO (Fig. 6b), B1-3DrGO (Fig. 6c) and B2-3DrGO (Fig. 6d) are positively shifted to  $-0.33$ ,  $-0.26$  and  $-0.18 \text{ V}$ , respectively. These are accompanied by a significant increase in the maximum peak currents for oxygen reduction:  $-1.25 \text{ mA cm}^{-2}$  for B-rGO,  $-1.18 \text{ mA cm}^{-2}$  for B1-3DrGO and  $-2.47 \text{ mA cm}^{-2}$  for B2-3DrGO. The CV results show that B-doping significantly improved the electrocatalytic activity towards ORR in terms of both the onset/peak potentials and the peak current. Furthermore, the electrocatalytic activities of catalysts for the ORR increase with increasing B content, and the highest activity was observed from the B2-3DrGO catalyst. The maximum peak current measured from the B2-3DrGO catalyst is 2.68, 1.98 and 2.09 times higher than that measured from 3DrGO, B-rGO, and B1-3DrGO, respectively.

To gain further insights into the role of B-3DrGO catalysts during the ORR process, linear sweep voltammetry measurements on the rotating disk electrode (RDE) were carried out for the B1-3DrGO and the B2-3DrGO catalysts. For comparisons, the 3DrGO, B-rGO and commercial Pt (20 wt.%) catalysts, were also tested

of commercial Pt/C. These results are consistent with the CV measurements and confirming, once again, that there is a significant improvement in the catalytic performance, originated from the B doping, in B-3DrGO with respect to 3DrGO. Though the electrocatalytic performance of our B-3DrGO is not as good as the commercial Pt/C (20 wt.%) catalyst (Figure 6e and 6f), there is a great potential for further development based on the method proposed in this paper for the synthesis of 3D porous graphene as a metal-free electrocatalyst toward ORR because this one-pot approach is simple and environmentally benign and that the product exhibits a high efficiency in the doping of heteroatoms and a large specific surface area.

In order to gain further insights into the electron transfer kinetics of the B-3DrGO during ORR, RDE measurements were performed in an  $O_2$ -saturated, 0.1 M KOH aqueous solution at various rotating speeds and a constant scan rate of  $10 \text{ mV s}^{-1}$ . The diffusion current densities ( $J$ ) of B1-3DrGO (Fig. S4a<sup>†</sup>), B2-3DrGO (Fig. 7a) and commercial Pt/C (Fig. S4b<sup>†</sup>) increase with the increasing of rotation rate ( $\omega$ ) from 225 to 2,500 rpm, while the onset potentials remain almost constant. The transferred electron number ( $n$ ) per oxygen molecule involved in the ORR process was determined by the Koutecky–Levich equation (see in Supporting Information).<sup>28,43</sup> The corresponding Koutecky–Levich plots ( $J^{-1}$  vs.  $\omega^{1/2}$ ) of B1-3DrGO (Fig. S4c<sup>†</sup>), B2-3DrGO (Fig. 7b) and commercial Pt/C (Fig. S4d<sup>†</sup>) at various electrode potentials exhibit a

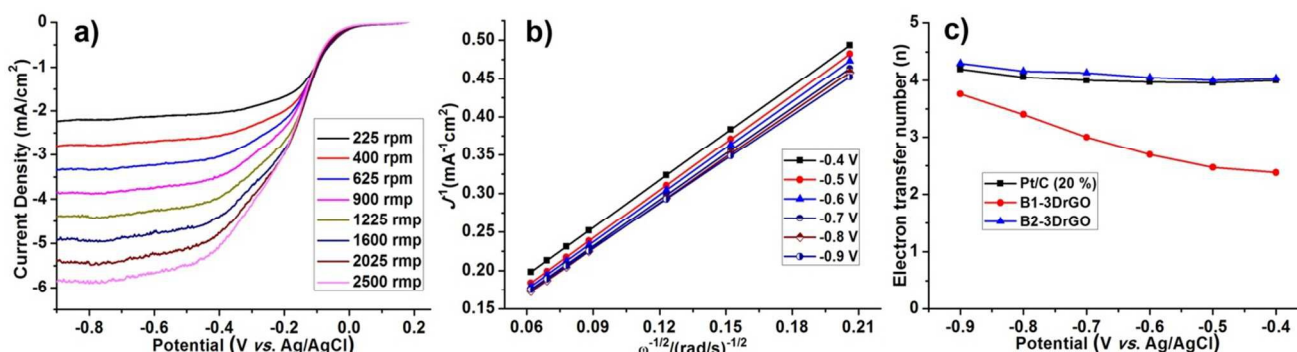


**Fig. 7.** (a) ORR polarization curves of B2-3DrGO in  $O_2$ -saturated 0.1 M KOH solution with various rotation rates at a scan rate of  $10 \text{ mV s}^{-1}$ . (b) Koutecky–Levich (K-L) plots of B2-3DrGO at different electrode potentials. The experimental data was shown in (a). (c) Electron-transfer number ( $n$ ) of B1-3DrGO, B2-3DrGO and commercial Pt/C (20 wt.%) at different potentials.

under the same experimental conditions. The voltammetric curves for different electrodes in an  $O_2$ -saturated 0.1 M KOH aqueous solution were obtained at the same rotation rate of 1,600 rpm and at a scan rate of  $10 \text{ mV s}^{-1}$ . As shown in Fig. 6f, two  $O_2$  reduction waves appear on the 3DrGO-modified electrodes. One of these waves refers to the two-electron reduction process of  $O_2$  to  $HO_2^-$ , and the other wave corresponds to the subsequent reduction of  $HO_2^-$  to  $OH^-$  in an alkaline medium. Only one reduction wave is observed in the B-doped graphene and the commercial Pt/C modified electrodes. Furthermore, the onset potential for oxygen reduction at the 3DrGO electrode is about  $-0.23 \text{ V}$ , which is positively shifted after B was doped into the rGO layers. The onset potentials for ORR at B-rGO, B1-3DrGO and B2-3DrGO catalysts are found to be at around  $-0.20$ ,  $-0.16$  and  $-0.05 \text{ V}$ , respectively. These values are all still smaller than that of the commercial Pt/C catalyst ( $-0.01 \text{ V}$ ). Moreover, the limiting diffusion current densities at  $-0.8 \text{ V}$  for the 3DrGO, B-rGO, B1-3DrGO and B2-3DrGO electrodes are  $-2.37$ ,  $-5.20$ ,  $-4.78$  and  $-0.4.97 \text{ mA cm}^{-2}$ , respectively. Obviously, B-3DrGO catalysts exhibit much higher electrocatalytic activity compared to the undoped 3DrGO. More importantly, B2-3DrGO shows the highest electrocatalytic activity amongst the others and is much closer to that

linear relationship, corresponding to a first-order reaction kinetics with respect to the concentration of dissolved  $O_2$ . As shown in Fig. 7c, the experimentally determined electron transfer number  $n$  is 4.06 at  $-0.8 \text{ V}$  for the commercial Pt/C. This value agrees well with the theoretically calculated value of  $n=4.0$ , indicating that it is a four-electron oxygen reduction process. The corresponding numbers of electrons transferred per  $O_2$  molecule at  $-0.8 \text{ V}$  for B1-3DrGO and B2-3DrGO are calculated to be 3.4 and 4.16, respectively. These values suggest that the ORR in the two catalysts is dominated by a four-electron process.

The electrochemical crossover effect and the stability are two important issues for cathode materials in fuel cells. The electrocatalytic selectivity of the B2-3DrGO against the electrooxidation of methanol was measured by CV in an  $O_2$ -saturated solution containing 0.1 M KOH solution and 1 M methanol. The commercial Pt/C electrode was used as a control and was tested under the same conditions. As presented in Fig. 8a, the cathodic signals toward the ORR that was detected at about  $-0.10 \text{ V}$  is not observed in the CV curve of the Pt/C electrode upon addition of methanol into the  $O_2$ -saturated 0.1 M KOH solution. The current intensity corresponding to methanol oxidation at the Pt/C electrode

at 0.03 eV increases significantly. However, no significant difference between the curves obtained with and without methanol can be observed in B2-3DrGO electrode (Fig. 8b), suggesting that the B2-3DrGO electrocatalyst is free from methanol poisoning. The above results clearly demonstrate that the metal-free B<sub>2</sub>-3DrGO catalyst not only possesses a high catalytic activity towards the ORR, but also has a much higher selectivity toward ORR than the commercial Pt/C electrocatalyst.

In addition to the crossover effect, the durability of B2-3DrGO and commercial Pt/C electrocatalysts were also studied and compared. CVs were obtained from the sample electrodes in O<sub>2</sub>-saturated 0.1 M KOH at a scan rate of 100 mV s<sup>-1</sup> from -1 to 0.2 V. For both samples, CVs from the first and the 2500<sup>th</sup> scanning cycles were compared. Fig. S5a shows the CVs of the B2-3DrGO electrode before and after 2,500 continuous cycles. A small decay of current and a negligible change in oxygen reduction peak were observed on the CV upon an extended cycling. On the contrary, a clear decay of current can be observed in the commercial Pt/C after 2,500 continuous cycles, (Fig. S5b, Supporting Information). The above results show that the B2-3DrGO product is more durable than the commercial Pt/C catalyst. Furthermore, only a 11.8 mV degradation can be seen in B2-3DrGO electrocatalyst (Fig. 8d) after 2,500 scanning cycles showed its durability is superior to that of Pt/C (40.0 mV) (Fig. 8c). These results indicate that the B2-3DrGO electrocatalyst has a much better electrochemical stability and durability than that of commercial Pt/C electrocatalyst.

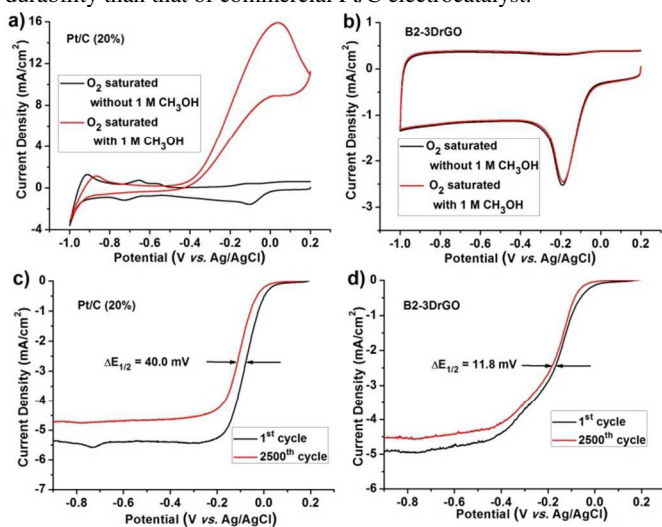


**Fig. 8.** CVs of samples on GC electrodes in O<sub>2</sub>-saturated 0.1 M KOH solution and O<sub>2</sub>-saturated 0.1 M solution of KOH upon addition of methanol (1 M) at a scan rate of 10 mV s<sup>-1</sup>. (a) commercial Pt/C (20 wt.%) and (b) B2-3DrGO. ORR polarization curves of (c) commercial Pt/C (20 wt.%) and (d) B2-3DrGO before and after 2500 scanning cycles in O<sub>2</sub>-saturated 0.1 M KOH at a scan rate of 100 mV s<sup>-1</sup>. The RDE test condition was set to a scan rate of 10 mV s<sup>-1</sup> at a fixed rotating speed of 1,600 rpm from -1 to 0.2 V.

#### 4. Conclusions

In summary, it is demonstrated that a hierarchically porous B-3DrGO can be produced using a green and simple one-pot technique with the use of ScCO<sub>2</sub>. The key was the complete miscibility of the selected reducers borane-THF or borane-N(C<sub>2</sub>H<sub>5</sub>)<sub>3</sub> and ScCO<sub>2</sub>, forming a single phase mixture under the conditions of 353 K and 300 atm. The low viscosity, high solvation power and high diffusivity characteristics of the SCFs allow them to be rapidly

diffused between the GO layers and then exfoliate them, forming a hierarchically porous structure. The reduction of GO sheets to rGO sheets by borane may also contribute to the observed hierarchically porous structure. As-prepared B-3DrGO using borane-THF possesses excellent properties including a high surface area due to its high porosity (541 m<sup>2</sup> g<sup>-1</sup>), a relatively high degree of reduction (C/O ratio is 5.9) and a high efficiency of B-doping (2.9 at%). The new products also demonstrate high ORR activities that is comparable to the commercially available Pt/C (20 wt.%) catalysts, but exhibit superior durability and resistance to the crossover effect. The results from this work suggests that the proposed one-pot synthesis technique with the use of ScCO<sub>2</sub> is a simple, green and promising synthesize method for heteroatoms doped 3D graphene, which may be used in a variety of energy conversion and storage applications.

#### Acknowledgements

YL and DD acknowledge the financial support from a WSU start-up grant. JY acknowledges the financial support from National Science Foundation of China (50902061).

#### Notes and references

<sup>a</sup> School of Mechanical and Materials Engineering, Washington State University, Pullman, WA 99164-2920, United States.

E-mail: Yuehe.lin@wsu.edu

<sup>b</sup> School of Materials Science and Engineering, Jiangsu University, Zhenjiang, 212013, Jiangsu, PR China.

E-mail: yangjuan6347@mail.ujs.edu.cn

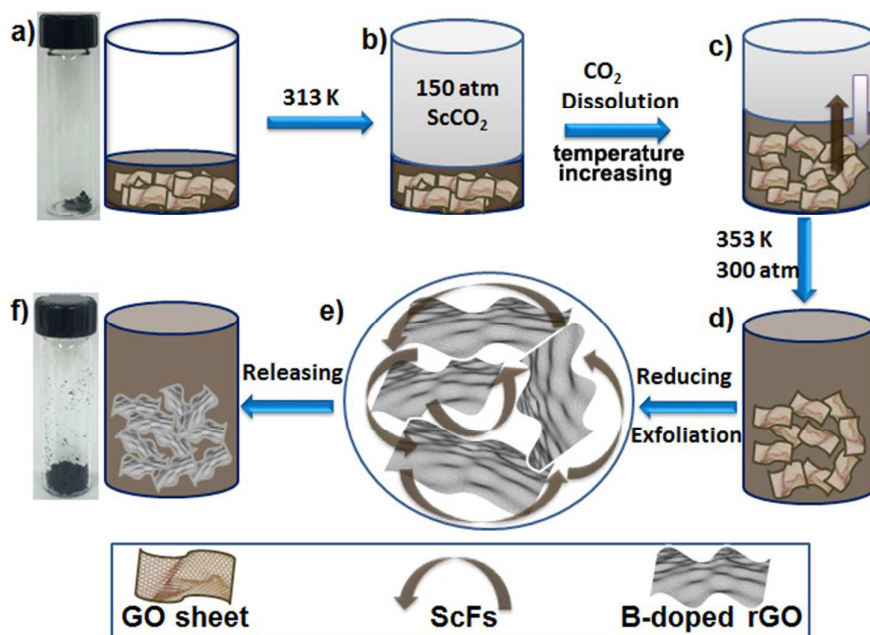
<sup>c</sup> Department of Chemistry, University of Idaho, Moscow, Idaho 83844-2343, United States.

† Electronic Supplementary Information (ESI) available: [SEM of B-3DrGO; N<sub>2</sub> adsorption/desorption measurement of B1-3DrGO product; XPS and electrochemical properties of B1-3DrGO and commercial Pt/C (20 wt.%) are available in supplementary information]. See DOI: 10.1039/b000000x/

- 1 A. K. Geim, *Science*, 2009, **342**, 1530-1534.
- 2 Z. Sui, Q. Meng, X. Zhang, R. Ma and B. Cao, *J. Mater. Chem.*, 2012, **22**, 8767-8771
- 3 Y. Zhu, S. Murali, M. D. Stoller, K. J. Ganesh, W. Cai, P. J. Ferreira, A. Pirkle, R. M. Wallace, K. A. Cychosz, M. Thommes, D. Su, E. A. Stach and R. S. Ruoff, *Science*, 2011, **332**, 1537.
- 4 X. Ma, G. Ning and Y. Sun, *Carbon*, 2014, **79**, 310-320.
- 5 H. Wang, K. Sun, F. Tao, D. J. Stacchiola and Y. H. Hu, *Angew. Chem. Int. Ed.*, 2013, **52**, 9210-9214.
- 6 Y. Wang, C. X. Guo, X. Wang, C. Guan, H. Yang, K. Wang and C. M. Li, *Energy Environ. Sci.*, 2011, **4**, 195-200.
- 7 W. He, C. Jiang, J. Wang and L. Lu, *Angew. Chem. Int. Ed.*, 2014, **53**, 9503-9507
- 8 Z. Chen, W. Ren, L. Gao, B. Liu and S. Pei, *Nat. Mater.*, 2011, **10**, 424-428.
- 9 T. Kobayashi, N. Kimura, J. Chi, S. Hirata and D. Hobarra, *Small*, 2010, **6**, 1210-1215.
- 10 S. Guo and S. Dong, *Chem. Soc. Rev.*, 2011, **40**, 2644-2672.
- 11 X. Huang, K. Qian, J. Yang, J. Zhang, L. Li, C. Yu, and D. Zhao, *Adv. Mater.*, 2012, **24**, 4419-4423.
- 12 Y. Long, C. Zhang, X. Wang, J. Gao, W. Wang and Y. Liu, *J. Mater. Chem.*, 2011, **21**, 13934-13941.

- 13 Y. Xu, K. Sheng, C. Li and G. Shi, *ACS Nano*, 2014, **4**, 4324-4330.
- 14 S. H. Lee, H. W. Kim, J. O. Hwang, W. J. Lee, J. Kwon, C. W. Bielawski, R. S. Ruoff and S. O. Kim, *Angew. Chem. Int. Ed.*, 2010, **49**, 10084-10088.
- 15 Z. Wu, A. Winter, L. Chen, Y. Sun, A. Turchanin, X. Feng and K. Müllen, *Adv. Mater.*, 2012, **24**, 5130-5135.
- 16 X. Wang, Y. Zhang, C. Zhi, X. Wang, D. Tang, Y. Xu, Q. Weng, X. Jiang, M. Mitome, D. Golberg and Y. Bando, *Nat Commun.*, 2013, **4**, 2905
- 17 S. Nardecchia, D. Carriazo, M. L. Ferrer, M. C. Gutierrez and F. del Monte, *Chem. Soc. Rev.*, 2013, **42**, 794-830
- 18 M. A. Worsley, P. J. Pauzauskie, T. Y. Olson, J. Biener, J. H. Satcher, Jr. and T. F. Baumann, *J. Am. Chem. Soc.*, 2010, **132**, 14067-14069.
- 19 Z. Zuo, Z. Jiang and A. Manthiram, *J. Mater. Chem. A*, 2013, **1**, 13476-13483.
- 20 K. P. Johnston and P. S. Shah, *Science*, 2004, **303**, 482-483.
- 21 F. M. Kerton, G. A. Lawless and S. P. Armes, *J. Mater. Chem.*, 1997, **7**, 1965-1966.
- 22 J. M. Blackburn, D. P. Long, A. Cabanas and J. J. Watkins, *Science*, 2001, **294**, 141-145.
- 23 A. I. Cooper, *Adv. Mater.*, 2003, **15**, 1049-1059.
- 24 D. Rangappa, D. Golberg, K. Sone, H. Itoh, M. Wang, M. Ichihara, U. K. Gautam and I. Honma, *Chem. Eur. J.*, 2010, **16**, 6488-6494
- 25 G. K. Serhatkulu, C. Dilek and E. Gulari, *J. Supercritical Fluids*, 2006, **39**, 264-270
- 26 L. Qu, Y. Liu, J. B. Baek and L. Dai, *ACS Nano*, 2014, **4**, 1321-1326.
- 27 Z. H. Sheng, H. L. Gao, W. J. Bao, F. B. Wang and X. H. Xia, *J. Mater. Chem.*, 2011, **22**, 390-395.
- 28 I. Y. Jeon, H. J. Choi, M. Choi, J. M. Seo, S. M. Jung, S. Zhang, L. Zhang, Z. Xia, L. Dai, N. Park, M. J. Kim and J. B. Baek, *Sci Rep.*, 2013, **3**, 180
- 29 Z. W. Liu, F. Peng, H. J. Wang, H. Yu, W. X. Zheng and J. Yang, *Angew. Chem. Int. Ed.*, 2011, **123**, 3315-3319.
- 30 Z. Yang, Z. Yao, G. Li, G. Fang, H. Nie, Z. Liu, X. Zhou, X. Chen and S. Huang, *ACS Nano*, 2011, **6**, 205-211.
- 31 S. Wang, L. Zhang, Z. Xia, A. Roy, D. W. Chang, J. B. Baek and L. Dai, *Angew. Chem. Int. Ed.*, 2012, **51**, 4209-4212.
- 32 a) K. Gong, F. Du, Z. Xia, M. Durstock and L. Dai, *Science*, 2009, **323**, 760-764; b) C. Zhu and S. Dong, *Nanoscale*, 2013, **5**, 1753-1767.
- 33 W. S. Hummers and R. E. Offeman, *J. Am. Chem. Soc.*, 1958, **80**, 1339.
- 34 J. Han, X. Zhao, L. Zhang, S. Lee, J. Oh, K. S. Lee, J. R. Potts, J. Ji, X. Zhao, R. S. Ruoff and S. Park, *ACS Nano.*, 2013, **7**, 19-26
- 35 R. A. Pai, R. Humayun, M. T. Schulberg, A. Sengupta and J. N. Sun, *Science*, 2004, **23**, **303**, 507-510
- 36 P. G. Jessop, Y. Hsiao, T. Ikariya and R. Noyori, *J. Am. Chem. Soc.*, 1996, **118**, 344-355.
- 37 Z. Knez, M. Skerget, L. Ili and C. Lutge, *J. Supercritical Fluids*, 2008, **43**, 383-389.
- 38 S. W. Cranford and M. J. Buehler, *Phys. Rev. B.*, 2011, **84**, 205451.
- 39 Y. Z. Zhou, J. Yang, T. T. He, H. F. Shi, X. N. Cheng and Y. X. Lu, *Small*, 2013, **9**, 3445-3454.
- 40 L. Ci, L. Song, C. Jin, D. Jariwala, D. Wu, Y. Li, A. Srivastava, Z. F. Wang, K. Storr, L. Balicas, F. Liu and P. M. Ajayan, *Nat. Mater.*, 2010, **9**, 430-435.
- 41 L. Yang, S. Jiang, Y. Zhao, L. Zhu, S. Chen, X. Wang, Q. Wu, J. Ma, Y. Ma, and Z. Hu, *Angew. Chem. Int. Ed.*, 2011, **50**, 7132-7135.
- 42 Y. Zhou, J. Yang, X. Cheng, N. Zhao, L. Sun, H. Sun, D. Li, *Carbon*, 2012, **50**, 4343-4350.
- 43 Y. Li, H. H. Cheng, Y. Hu, G. Q. Shi, L. M. Dai and L. T. Qu, *J. Am. Chem. Soc.*, 2012, **134**, 15-18.

## Table of Contents Entry



Supercritical carbon dioxide technique, a one-pot method, was used to synthesize B-doped 3D reduced graphene oxide. The good electrochemical properties demonstrated that it is a good electrocatalyst for oxygen reduction reaction.